J|A|C|S ARTICLES

Published on Web 05/28/2010

Intramolecular Catalysis of Phosphodiester Hydrolysis by Two Imidazoles

Elisa S. Orth,[†] Tiago A. S. Brandão,[†] Bruno S. Souza,[†] Josefredo R. Pliego,[‡] Boniek G. Vaz,[§] Marcos N. Eberlin,[§] Anthony J. Kirby,*[,||] and Faruk Nome*[,†]

INCT-Catálise, Departamento de Química, Universidade Federal de Santa Catarina, Florianópolis, Santa Catarina 88040-900, Brazil, Universidade Federal de São João Del-Rei, Sao Joao Del Rei, MG, 36301-160, Brazil, ThoMSon Mass Spectrometry Laboratory, Institute of Chemistry, University of Campinas-UNICAMP, Campinas, SP, Brazil 88040-900, and University Chemical Laboratory, Cambridge CB2 1EW, U.K.

Received April 23, 2010; E-mail: faruk@qmc.ufsc.br

Abstract: Two imidazole groups act together to catalyze the hydrolysis of the phosphodiester bis(2-(1-methyl-1*H*-imidazolyl)phenyl) phosphate (**BMIPP**). A full investigation involving searching computational and electrospray ionization (ESI-MS-/MS) and ultra mass spectrometry (LTQ-FT) experiments made possible a choice between two kinetically equivalent mechanisms. The preferred pathway, involving intramolecular nucleophilic catalysis by imidazole, assisted by intramolecular general acid catalysis by the imidazolium group, offers the first simple model for the mechanism used by the extensive phospholipase D superfamily.

Introduction

Relatively few enzymes are capable of cleaving a P−OR bond of an unactivated phosphodiester without the aid of a metal. So those known to do so—and their number is growing—are of particular interest. The key to a successful substitution reaction at an unreactive phosphorus center is always the delivery of the primary nucleophile. In the familiar ribonuclease mechanism this is the neighboring 2′-OH group of the substrate, but otherwise, in the absence of a metal cation, this is typically a nucleophilic group from an active-site amino acid. In enzymes belonging to the extensive phospholipase D superfamily, the nucleophile is a histidine imidazole, thought to be assisted by a second imidazole properly positioned by the extensive common sequence motif, $HisXLys(X)_4Asp(X)_6GlySerXAsn$, which occurs twice in the (typically dual-domain or dimeric) holoenzyme.[1−3] In the topoisomerases the nucleophile is the hydroxyl oxygen of a tyrosine, but the hydrolysis of the intermediate protein-tyrosine phosphate diester thus formed, at the 3′-terminus of the DNA chain, is itself catalyzed by a phospholipase D superfamily enzyme.[4]

The mechanism suggested for this group of enzymes (specifically for the "ubiquitous acid endonuclease" DNase II[5]) is outlined in Scheme 1. It involves a (presumably concerted) $S_N2(P)$ reaction in which nucleophilic attack is assisted by what is effectively general acid catalysis of the departure of the leaving group.

Scheme 1[a]

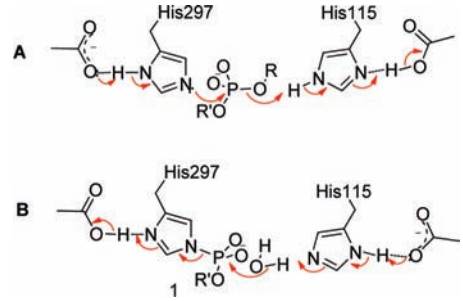

[a] (A) Enzymes of the phospholipase D superfamily use two active site histidines to catalyze the cleavage of unreactive phosphodiesters by a nucleophilic mechanism involving a phosphoryl-enzyme intermediate **1**. (B) The intermediate is rapidly hydrolyzed by the reverse of the cleavage mechanism, with water replacing the departing nucleotide ROH.

No simple model is available for this mechanism. We have characterized intramolecular general acid catalysis (IGAC) by the imidazolium group in the hydrolysis of the phosphate monoester **2** as moderately efficient, by virtue of the intramolecular hydrogen bond stabilizing the product **3** and the transition state leading to it (Scheme 2).[6]

We also identified efficient IGAC of the attack of nitrogen nucleophiles on phosphodiester phosphorus in system **4**, which was designed specifically to generate a strong intramolecular H-bond in the product **5**, and thus also in the transition state leading to it. The pK_a of the general acid in **4** is 7.4, close to that of imidazole.

[†] Universidade Federal de Santa Catarina.
[‡] Universidade Federal de São João Del-Rei.
[§] University of Campinas-UNICAMP.
[||] University Chemical Laboratory.

(1) Gottlin, E. B.; Rudolph, A. E.; Zhao, Y.; Matthews, H. R.; Dixon, J. E. *Proc. Natl. Acad. Sci. U.S.A.* **1998**, *95*, 9202–9207.
(2) Stuckey, J. A.; Dixon, J. E. *Nat. Struct. Biol.* **1999**, *6*, 278–284.
(3) Exton, J. H. *Rev. Physiol., Biochem. Pharmacol.* **2002**, *144*, 1–94.
(4) Interthal, H.; Pouliot, J. J.; Champoux, J. J. *Proc. Natl. Acad. Sci. U.S.A.* **2001**, *98*, 12009–12014.
(5) Cheng, Y.-C.; Hsueh, C.-C.; Lu, S.-C.; Liao, T.-H. *Biochem. J.* **2006**, *398*, 177–185.
(6) Brandão, T. A. S.; Orth, E. S.; Rocha, W. R.; Bortoluzzi, A. J.; Bunton, C. A.; Nome, F. *J. Org. Chem.* **2007**, *72*, 3800–3807.

Scheme 2. Mechanism of Intramolecular General Acid Catalysis of the Hydrolysis of Phosphate Monoester **2**[6]

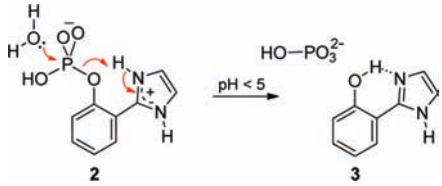

Because of the extended, linear geometry of the nucleophile···P···OR system in the transition state (Scheme 1), the only way to introduce a neutral imidazole as a second catalytic group into a simple diester based on **4** is to attach into the second ("spectator") ester group (e.g., the OMe in **4**). Introducing a neighboring imidazole in this way into **2** gave the system **BMIPP** (bis(2-(1-methyl-1*H*-imidazolyl)phenyl) phosphate),

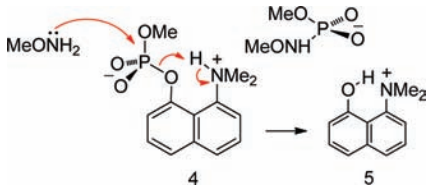

which, like enzyme active sites deploying two histidines, has two catalytic groups in potentially productive proximity of the unreactive phosphodiester center. We found[7] that **BMIPP** is hydrolyzed approximately 10^7 times faster than expected for a simple diaryl phosphate with leaving groups of similar pK_a (~ 7.85[8]), although this value is considerably higher when compared with diphenyl phosphate (vide infra). To account for this high reactivity we suggested the mechanism shown as path **A** in Scheme 3, involving IGAC of intramolecular general base catalysis (IGBC), and making the reaction formally a model for the mechanism used by RNase A.[7]

However, the substantial combined effect of the two catalytic groups could also be explained in terms of (the kinetically equivalent) intramolecular nucleophilic catalysis (NUC) by the neighboring imidazole free base, concerted with the expected efficient IGAC (Scheme 3, path **B**). In the absence of a steric or stereoelectronic barrier, intramolecular nucleophilic catalysis is reliably more efficient than IGBC, with effective molarities of up to 10^9 in conformationally flexible systems, compared with a limit of about 60 M for IGBC, which has still not been surpassed.[9] This limit applies in particular to all known model

Scheme 3. Alternative Mechanisms for the Rapid Hydrolysis of the Phosphodiester **BMIPP**, Involving Intramolecular General Acid Catalysis (IGAC) by the Imidazolium Group of General Base (Path **A**) or Nucleophilic Catalysis (Path **B**) by the Imidazole Free Base

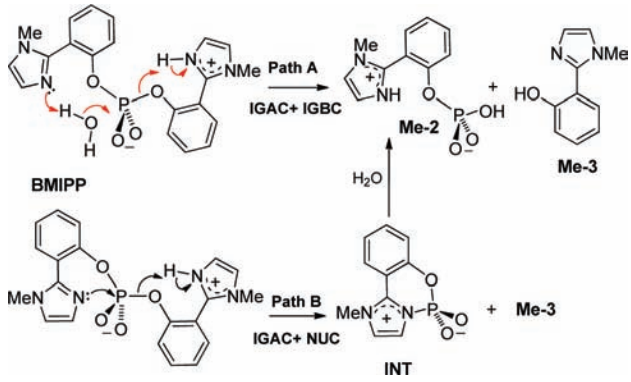

systems involving water as the primary nucleophile, and the mechanisms by which enzymes activate water so effectively in the absence of a metal remain an important challenge for model design.[10] RNA, and successful systems designed to model the ribonuclease mechanism, has a nucleophilic OH group built in (with EM ≈ 10^7 M in the reactions of ribose derivatives[9]).

We report new experimental and computational evidence from a detailed investigation of the hydrolysis of the diester **BMIPP**, which includes the identification of the imidazolium derivative **INT** as a short-lived intermediate, thus defining our preferred mechanism as intramolecular nucleophilic catalysis, concerted with IGAC of the departure of the leaving group by the second, imidazolium group (path **B** in Scheme 3).

Results and Discussion

Kinetics. pH−rate profiles for the hydrolysis of the diester **BMIPP** and the corresponding monoester 2-(1-methyl-2′-imidazolium)phenyl phosphate (**Me-2**) are compared with previous results for the nonmethylated monoester 2-(2′-imidazolium)phenyl phosphate (**2**)[6] in Figure 1. The bell-shaped profile for **BMIPP** shows a rate maximum at pH 6.6−6.8, indicating bifunctional catalysis, involving both protonated and neutral imidazole groups of the zwitterionic species (**BMIPP**$^{\pm}$).

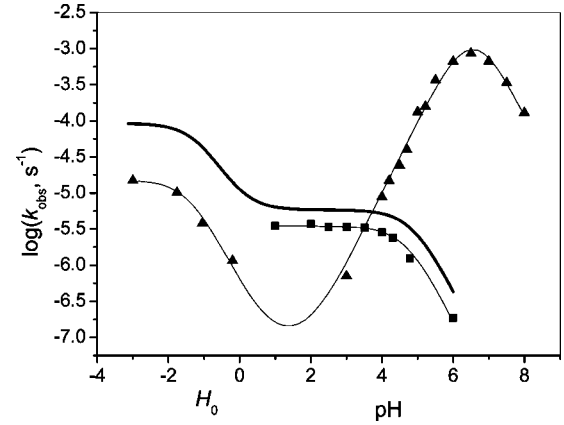

Figure 1. pH−rate profiles for the hydrolysis of **BMIPP** (▲) and **Me-2** (■), at 60 °C, I = 1.0 (KCl). The solid lines for **BMIPP** and **Me-2** represent fits with eq 1. The bold curve shows the corresponding fit for hydrolysis of 2-(2′-imidazolium)phenyl phosphate (**2**) at 60 °C, I = 1.0 (KCl).[6]

Direct titration of **BMIPP** gave consistent pK_a values for the imidazole groups of pK_{a2} = 6.2 and pK_{a3} = 7.8. (Rate and dissociation constants are defined in Scheme 4.)

The data for **BMIPP** and **Me-2** in Figure 1 were fitted to eq 1, based in Scheme 4.

$$k_{obs} = k_{1d}\chi_{1d} + k_{2d} + k_{3d}\chi_{3d} + k_{4d}\chi_{4d} \qquad (1)$$

The rate constants k_{1d}, k_{2d}, k_{3d}, and k_{4d} refer to the hydrolysis of individual ionic species of **BMIPP**. The molar fractions χ_{1d}, χ_{2d}, χ_{3d}, and χ_{4d} represent the dicationic, monocationic, zwitterionic, and anionic **BMIPP** species, respectively. A similar equation was used to analyze the results for monoesters **2** and **Me-2**, and the subscript for molar fractions and rate constants is m (Scheme 4). K_{a1} is the dissociation constant for the phosphoric acid group and is estimated from kinetic data in the acidic (h_0) range as approximately −1.5, consistent with values assigned by other authors to similar phosphate esters.[6,11] K_{a2} and K_{a3} (Scheme 4) are the dissociation constants of the phosphoryl and imidazole groups of **Me-2** and **BMIPP**,

Scheme 4. Rate and Equilibrium Constants Accounting for the Hydrolysis of **BMIPP** over the pH Range[a]

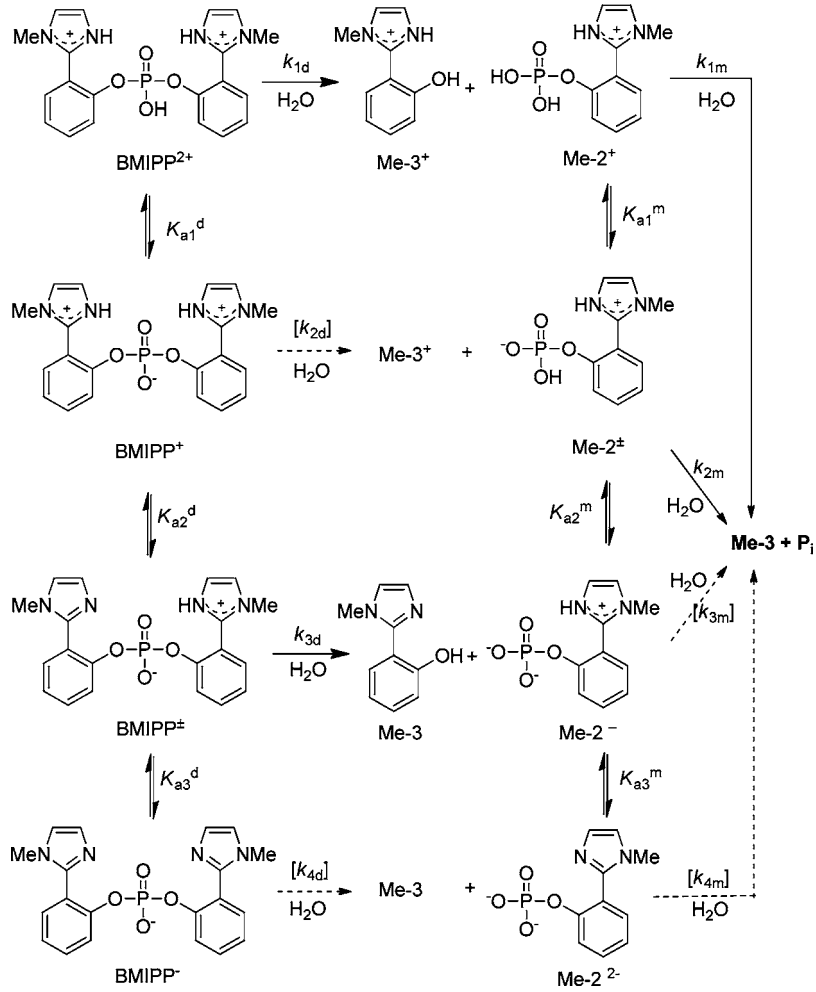

[a] The dashed arrows represent reactions too slow to be observed in this work.

respectively. The rate constants k_{2d} and k_{4d} in the diester hydrolysis and k_{3m} and k_{4m} in the monoester reactions refer to extremely slow reactions, which were not detected experimentally, so were neglected in the fitting.

The kinetic parameters obtained by fitting the data in Figure 1 are presented in Table 1, and compared with previous results reported for **2**, all according to eq 1.[6] The dissociation constants pK_{a2} and pK_{a3} are from titration measurements for **BMIPP** and **2**, while pK_{a2} for **Me-2** was estimated from the kinetic results. The result is consistent with the value obtained for **2**.

Hydrolysis in Acid. Acid catalysis in the H_0 region (Hammett's acidity function, $H_0 = -\log h_0$)[13] corresponds to the reaction of the dication **BMIPP**$^{2+}$. The developing rate maximum at $H_0 \approx -2$, and the similar behavior of **2** in the same region, is observed for the reactions of many aryl and naphthyl phosphate esters which involve the attack of a water molecule in the rate-limiting step. Values of k_{obs} in the H_0 region of Figure 1 have been corrected for water activity (k_{obs}/a_w).[12] Further evaluation of the acid hydrolysis of **BMIPP**$^{2+}$ gave Bunnett parameters w and Φ (calculated from eq 2 and 3: for data see Supporting Information) of $w = 9.6$ ($n = 4$, $R = 0.979$) and $\Phi = 0.98$ ($n = 4$, $R = 0.979$). These are similar to the values estimated for the acid hydrolysis of **2** ($w = 11.6$, $\varphi = 1.31$, $n = 7$, $R = 0.998$),[6] 8-(*N*,*N*-dimethylamino)-1-naphthyl phosphates ($w = 10.9$, $\varphi = 1.18$, $n = 12$, $R = 0.997$),[14] and other aryl phosphate esters ($w \approx 7$, $\varphi \approx 1.2$)[15] where the suggested

Table 1. Kinetic Parameters[a,b] Compared for the Hydrolysis of Phosphodiester **BMIPP** and Monoesters **2** and **Me-2**, at 60 °C

	BMIPP	2[6]	Me-2
k_1, s^{-1}	$(1.52 \pm 0.11) \times 10^{-5}$	$(8.67 \pm 0.57) \times 10^{-5}$	—
k_2, s^{-1}	—	$(5.83 \pm 0.18) \times 10^{-6}$	$(3.65 \pm 0.06) \times 10^{-6}$
k_3, s^{-1}	$(1.98 \pm 0.13) \times 10^{-3}$	—	—
pK_{a1}	-1.42 ± 0.05[c]	-1.17 ± 0.16[c]	—
pK_{a2}	6.10 ± 0.04[d]	4.67 ± 0.02[d]	4.52 ± 0.03[c]
pK_{a3}	7.80 ± 0.05[d]	7.43 ± 0.04[d]	—

[a] The equations used for fitting **BMIPP** (eq S3) and **Me-2** (eq S4), are given in full in the Supporting Information. [b] k_{obs} values in the H_0 region have been corrected for water activity (k_{obs}/a_w).[12] [c] Estimated kinetically at 60 °C. [d] Determined by potentiometric titrations at 25 °C. The corresponding values calculated from the kinetic fit are p$K_{a2} = 6.12$ and p$K_{a3} = 6.98$ for **BMIPP** and p$K_{a2} = 4.90$ and p$K_{a3} = 7.47$ for **2**.[6]

(7) Orth, E. S.; Brandao, T. A. S.; Milagre, H. M. S.; Eberlin, M. N.; Nome, F. *J. Am. Chem. Soc.* **2008**, *130*, 2436–2437.
(8) Rogers, G. A.; Bruice, T. C. *J. Am. Chem. Soc.* **1974**, *96*, 2463–2472.
(9) Kirby, A. J. *Adv. Phys. Org. Chem.* **1980**, *17*, 183–278.
(10) Kirby, A. J.; Medeiros, M.; Oliveira, P. S. M.; Brandao, T. A. S.; Nome, F. *Chem.—Eur. J.* **2009**, *15*, 8475–8479.
(11) Kirby, A. J.; Lima, M. F.; Silva, D.; Roussex, C. D.; Nome, F. *J. Am. Chem. Soc.* **2006**, *128*, 16944–16952.
(12) Åkerlof, G.; Teare, J. W. *J. Am. Chem. Soc.* **1937**, *59*, 1855–1869.
(13) Anslyn, E. V.; Dougherty, D. A. *Modern Physical Organic Chemistry*; University Science Books: Sausalito, CA, 2006.

Table 2. Efficiency of Intramolecular Catalysis of Phosphate Ester Hydrolysis[a]

Reaction	k_{cat}/k_{noncat}	k_H/k_D
Bifunctional intramolecular catalysis in the hydrolysis of **BMIPP**$^{\pm}$	10^{11}	1.42
Intramolecular general acid catalysis in the hydrolysis of **BMIPP**$^{2+}$	10^{7}	–
Intramolecular nucleophilic-general acid catalysis in the hydrolysis of **7**[20]	10^{10}	–
Intramolecular nucleophilic and general acid catalysis in the hydrolysis of **8**[21]	10^{8}	1.9
Intramolecular general acid catalysis in the hydrolysis of **2**[6]	10^{9}	1.0
Intramolecular general acid catalysis in the hydrolysis of **6**[14]	10^{8}	1.46
Intramolecular general acid catalysis in the hydrolysis of **4**[11]	10^{9}	1.72
Bifunctional general acid−base catalysis by β-cyclodextrin bis-imidazole in the hydrolysis of 4-*tert*-butylcatechol cyclic phosphate[19]	120	2.12

[a] Efficiency (k_{cat}/k_{noncat}) was calculated by comparing with the hydrolysis of diphenyl phosphate ($k_{H_2O} = 1.54 \times 10^{-14}$ s^{-1} at 60 °C; applying Arrhenius equation[22]).[23] In the case of β-cyclodextrin bis-imidazole, efficiency was calculated by comparing with the spontaneous hydrolysis reaction of 4-*tert*-butylcatechol cyclic phosphate.

hydrolysis mechanism involves slow proton transfer concerted with water attack.[16]

$$\log k_{obs} + H_0 = w \log a_w + \text{constant} \quad (2)$$

$$\log k_{obs} + H_0 = \phi(H_0 + \log[HCl]) + \text{constant} \quad (3)$$

The hydrolysis mechanism suggested for **BMIPP**$^{2+}$ in the H_0 region is shown in Scheme 5, together with that proposed for the reaction of **2** (from Scheme 2),[6] where the departure of the leaving group is assisted by general acid catalysis by the protonated imidazole group as a water molecule attacks the phosphorus atom. The same mechanism should apply also to the hydrolysis of **Me-2**, although experimental data in the acid region were not obtained for this ester, which was studied specifically for comparison with the reaction of the reactive species **BMIPP**$^{\pm}$ at pH > 6. Acid catalysis is also very efficient in the hydrolysis of **BMIPP**$^{2+}$, with an estimated rate enhancement of $>10^5$ compared to phosphate esters without the neighboring general acid.[17] Upon comparison of the acid hydrolysis (k_1) constants in Table 1, the diester **BMIPP**$^{2+}$ is observed to be approximately 8 times less reactive than monoester **2**$^{+}$, which shows one of the most efficient general acid catalyzed reactions reported in the literature.[6] This reduced reactivity may result from a steric effect of the methyl group in **BMIPP**$^{2+}$, impeding the optimal conformation necessary for the acid catalysis possible for **2**$^{+}$ (Scheme 5). There is no evidence for the formation of a pentacovalent addition intermediate, proposed for acid hydrolyses of some phosphate esters,[18] perhaps for steric reasons. In fact computational results for **2** strongly disfavor this mechanism,[6] a conclusion which should apply to **BMIPP**$^{2+}$ also.

Scheme 5. Suggested Mechanism for the Hydrolysis of **BMIPP**$^{2+}$ in Strong Acid, Compared with the Similar Reaction of **2**[6] (See the Text)

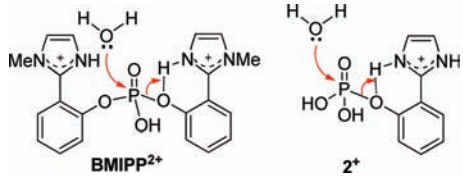

Bifunctional Catalysis near pH 7. The most reactive diester species, **BMIPP**$^{\pm}$, is hydrolyzed over 100 times faster than **BMIPP**$^{2+}$. This suggests an important catalytic role for the neutral imidazole, acting as a general base or nucleophile (Scheme 3). Comparing hydrolysis rate constants (Table 1: k_2 for **2** and **Me-2**; k_3 for **BMIPP**$^{\pm}$) for the zwitterionic species of the esters shown in Figure 1 shows that **Me-2** is a little less reactive than **2**: presumably the *N*-methyl group decreases the planarity of the arylimidazole aromatic system and, therefore, reduces the catalytic efficiency of the imidazolium general acid. On the other hand, the zwitterionic species **BMIPP**$^{\pm}$ is hydrolyzed appreciably faster, by a factor of up to 540, than the corresponding monoester **Me-2**. Phosphate monoesters, including systems set up for IGAC, are generally more reactive than the corresponding diesters: thus the monoester (**6**) derived from 8-dimethylamino-1-naphthyl phosphate is hydrolyzed 18 times faster at 60 °C than the corresponding diester (**4**).[11] The enhanced reactivity of **BMIPP**$^{\pm}$ compared to **Me-2** substantiates the importance of the additional imidazole free base in what must therefore be bifunctional catalysis.

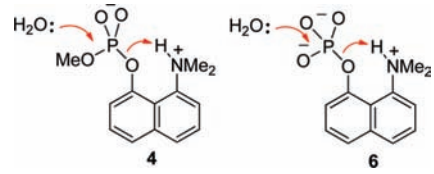

This bifunctional intramolecular catalysis could involve general acid assistance to either general base or nucleophilic catalysis, since the two pathways (**A** and **B** in Scheme 3) are kinetically equivalent. To compare the catalytic efficiency of other intramolecular catalytic systems with that shown by **BMIPP**, we adopted as a comparison standard the hydrolysis reaction of diphenyl phosphate in the absence of catalysis, which is one of the most common phosphate esters used for comparison purposes in the literature, Table 2. Bifunctional general acid−base catalysis by β-cyclodextrin bis-imidazole in the hydrolysis of 4-*tert*-butylcatechol cyclic phosphate is by far less efficient than the intramolecular systems and shows a higher isotope effect.[19] Intramolecular catalysis in the case of **BMIPP**$^{\pm}$ stands among the most efficient: it is hydrolyzed at approximately the same rate (half-life of 5.83 min at 60 °C) as the two efficient systems **7** and **8**, based on two carboxy groups, which are hydrolyzed with half-lives of 6.42 and 10.2 min at 50 and 39 °C, respectively. All three phosphodiesters show pH-rate maxima, but for the dicarboxy compounds **7** and **8** these are near pH 4.[20,21] The balance between the contributions of the two catalytic groups is expected to change, since the nucleophile is weaker

(14) Kirby, A. J.; Dutta-Roy, N.; Silva, D.; Goodman, J. M.; Lima, M. F.; Roussev, C. D.; Nome, F. *J. Am. Chem. Soc.* **2005**, *127*, 7033–7040.
(15) Bunton, C. A.; Farber, S. J. *J. Org. Chem.* **1969**, *34*, 767–772.
(16) Bunnett, J. F. *J. Am. Chem. Soc.* **1961**, *83*, 4956–4967.
(17) Kirby, A. J.; Younas, M. *J. Chem. Soc. B* **1970**, 1165–1172.
(18) Bunton, C. A. *Acc. Chem. Res.* **1970**, *3*, 257–265.
(19) Breslow, R.; Schmuck, C. *J. Am. Chem. Soc.* **1996**, *118*, 6601–6605.

Table 3. Kinetic Parameters for the Hydrolysis of **BMIPP**, Derived from Data for k_{obs} Measured between pH 5.5−8.0 (See Supporting Information)

Conditions	k_3 10^{-3} s^{-1}	pK_{a2}[a]	pK_{a3}[a]
50 °C, H_2O	0.77	6.24	6.99
60 °C, H_2O	1.98	6.12	6.98
70 °C, H_2O	3.52	5.80	6.83
80 °C, H_2O	7.15	5.58	6.79
60 °C, D_2O	1.39	6.91	7.51

[a] Values of pK_{a2} and pK_{a3} were estimated from the fit of the kinetic data at each temperature.

in the case of the less basic carboxylate, but the COOH a correspondingly stronger general acid. The acyl phosphates produced by the initial nucleophilic attack have been identified as intermediates in the reactions of **7** and **8**,[20,21] so the involvement of the stronger, imidazole, nucleophile in a system with almost identical geometry and closely similar leaving group would not be surprising.

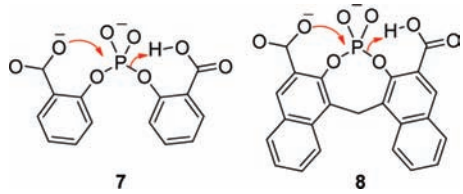

7 **8**

Kinetic Isotope Effect and Thermodynamic Parameters. The hydrolysis of the zwitterionic species **BMIPP**$^{\pm}$ is characterized by a low deuterium isotope effect, $k_{H_2O}/k_{D_2O} = 1.42$ (data from Table 3), consistent with a single proton transfer in the transition state for the bifunctional intramolecular catalysis.[6,24] Low values close to unity are expected for the nucleophilic part of the mechanism (e.g., $k_H/k_D = 1.10$ for the hydrolysis of 2-carboxyphenyl-3-nitrophenyl phosphate, which involves nucleophilic intramolecular catalysis by carboxylate[25]) but are observed also for various reactions involving intramolecular general acid catalysis of the hydrolysis of phosphate diesters (Table 2). Thus $k_H/k_D \approx 1.70$ for the hydrolysis of **4**,[11] where the dimethylammonium center promotes efficient intramolecular acid catalysis, and $k_H/k_D = 1.9$ for the hydrolysis of the anion of **8**, which involves bifunctional nucleophilic-general acid catalysis by the two carboxy groups.[21] The kinetic isotope effect, $k_{H_2O}/k_{D_2O} = 1.42$, observed for the hydrolysis of **BMIPP**$^{\pm}$, is consistent, though not uniquely consistent, with the bifunctional nucleophilic-general acid catalysis mechanism and so is not of itself sufficient evidence to rule out the mechanism (path **A** in Scheme 3) involving two rather than one proton transfers in the rate-determining transition state.

The activation parameters calculated for the hydrolysis of **BMIPP**$^{\pm}$, with the rate constants given in Table 3, are $\Delta H^{\ddagger} = 19.0 \pm 1.2$ kcal/mol and $\Delta S^{\ddagger} = -9.05 \pm 0.5$ e.u., giving a Gibbs free energy, calculated at 25 °C, of 21.7 ± 1.4 kcal mol^{-1}. In principle, entropy values close to zero are expected for unimolecular reactions,[25] and values close to −25 e.u. are commonly observed for bimolecular reactions:[15] but these are guidelines rather than rules. Thus $\Delta S^{\ddagger}$ values of −3.9 e.u. and −14.4 e.u. have been observed in relevant unimolecular intramolecular nucleophilic reactions;[21,25] and the formally bimolecular reactions of methyl 8-dimethylamino-1-naphthyl phosphate with water ($\Delta S^{\ddagger} = -12.0$ e.u) and three other nucleophiles ($\Delta S^{\ddagger} = 18.8-24.8$ e.u.) differ significantly.[11] Thus $\Delta S^{\ddagger} = -9.05 \pm 0.5$ e.u. also is consistent, but not uniquely consistent, with the bifunctional nucleophilic−general acid catalysis mechanism for the hydrolysis of **BMIPP**$^{\pm}$. A triester-like mechanism involving protonation of a nonbridging oxygen[26] can be ruled out in the hydrolysis of **BMIPP**$^{\pm}$, since such catalysis is known to cause small rate enhancements.[26]

Buffer Catalysis. The much higher EMs typically observed for intramolecular nucleophilic catalysis[9] mean that reactions with the limited concentrations of external nucleophiles available in solution cannot compete. So a simple but reliable test of mechanism which is the presence or absence of such catalysis was carried out. The hydrolysis reactions of phosphate esters are often strongly accelerated in the presence of external nucleophiles, especially the exceptionally reactive α-nucleophiles. For example, cleavage of bis(2,4-dinitrophenyl) phosphate is 10^4-fold faster,[27] and the reaction of the triester diethyl 8-(*N*,*N*-dimethylamino)-1-naphthyl phosphate is 10^5-fold faster in the presence of 0.5 M hydroxylamine, compared with the reactions with water.[28] We find that the rate of disappearance of **BMIPP** is not affected by added 1 M acetate, 1 M imidazole, or even the α-nucleophile hydroxylamine (also 1M), over the pH range 4−8 at 60 °C. Fitting the data to eq 1 gives values for k_3 identical within experimental error ($<1.3 \times 10^{-4}$) to that obtained previously (Table 1). (For details see Figure S8 and Tables S9−S10 of the Supporting Information.) This is prima facie evidence against the IGBC-IGAC mechanism (path **A** of Scheme 3), unless the intramolecular general base catalysis shows unprecedented efficiency.

Product Characterization by NMR. ^1H and ^{31}P NMR spectra taken at regular time intervals during the course of **BMIPP** hydrolysis in D_2O are shown in Figures 10 and 11 in the Experimental Section. Three species were observed: **BMIPP**, which gives the stable phenol product **Me-3** plus the monoester **Me-2** as an intermediate, which is itself hydrolyzed more slowly to a second molecule of **Me-3** and inorganic phosphate.

Figure 2 shows relative concentrations of the three compounds measured by ^{31}P NMR as they appear or disappear during the course of the reaction. The solid curves in the figure represent fits to a consecutive-reaction model. The derived rate constants (k_{obs}) for the hydrolysis of **BMIPP** at pD 7.2 and of **Me-2** at pD 1.5 are 3.0×10^{-4} and 2.7×10^{-6} s^{-1}, respectively.

Computational Calculations. To better understand the structures and likely behavior of reactants, transition states, and possible intermediates in the reaction path leading from **BMIPP**$^{\pm}$ to **Me-2** and **Me-3**, we performed computational calculations at the B3LYP level to compare the two mechanisms described in Scheme 3: intramolecular general base catalysis of the attack of a water molecule on phosphorus (path **A**) and intramolecular nucleophilic attack of the imidazole group on

(20) Kirby, A. J.; Abell, K. W. Y. *J. Chem. Soc., Perkin Trans. 2* **1983**, *8*, 1171–1174.
(21) Bruice, T. C.; Blaskó, A.; Arasasingham, R. D.; Kim, J. S. *J. Am. Chem. Soc.* **1995**, *117*, 12070–12077.
(22) Jencks, P. J. *Catalysis in Chemistry and Enzymology*; Dover Publications, Inc.: New York, 1987.
(23) Kirby, A. J.; Younas, M. *J. Chem. Soc. B* **1970**, 510–513.
(24) Khan, S. A.; Kirby, A. J. *J. Chem. Soc. B* **1970**, 1172–1182.
(25) Khan, S. A.; Kirby, A. J.; Wakselman, M. *J. Chem. Soc. B* **1970**, 1182–1187.
(26) Anslyn, E. V.; Piatek, A. M.; Gray, M. *J. Am. Chem. Soc.* **2004**, *126*, 9878–9879.
(27) Domingos, J. B.; Longhinotti, E.; Bunton, C. A.; Nome, F. *J. Org. Chem.* **2003**, *68*, 7051–7058.
(28) Kirby, A. J.; Tondo, D. W.; Medeiros, M.; Souza, B. S.; Priebe, J. P.; Lima, M. F.; Nome, F. *J. Am. Chem. Soc.* **2009**, *131*, 2023–2028.

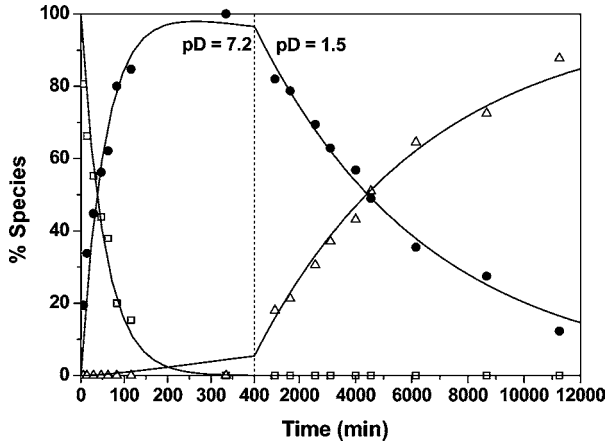

Figure 2. Relative species concentrations, obtained from repeated ^{31}P NMR scans over time, for hydrolysis of **BMIPP** at pD 7.2 and **Me-2** at pD 1.5, in D_2O at 60 °C: (□) **BMIPP**, (●) **Me-2**, (△) $\mathbf{P_i}$.

phosphorus, also with a water molecule present (path **B**). Tables of Cartesian coordinates and thermochemistry data appear in full in section 3 of the Supporting Information.

In both cases, the first step should be the solvation of the phosphate zwitterion. Although there is a strong interaction between O3 and the neighboring imidazolium group, which partially neutralizes the phosphate negative charge, **BMIPP**$^{\pm}$ interacts favorably with the water molecule through the N1 atom of the imidazole group and O2, to form the organic phosphate−water complex **BMIPP**$^{\pm}$**.w** (Figure 3). This interaction has a ΔG_{eq} of −2.78 kcal·mol^{-1}, thus **BMIPP**$^{\pm}$**.w** is taken to be the reacting species. The use of the gas phase to simplify the computational calculations is reinforced by the fact that the addition of the ΔG^{solv} term, computed by single-point calculations using PCM, gives very similar results and the free energies differences are not affected to a large extent (see sections 3.1 and 3.2 of the Supporting Information). Therefore, all structures and thermodynamic parameters presented here are computed in the gas phase, without the inclusion of the ΔG^{solv} term.

Table 4. Selected Distances (Å) and Angles (deg) for Optimized Structures of **BMIPP**$^{\pm}$**.w**, **TS.GB**, **TS.NUC**, and **TS.NUC2**[a,b]

	BMIPP$^{\pm}$.w	TS.GB	TS.NUC	TS.NUC2
O3−H1	1.50	2.56	1.68	1.67
O4−P	1.70	2.32	2.32	2.32
O4−H1	2.50	1.66	2.26	2.27
O5−P	4.02	2.20	3.78	−
N1−H2	2.19	1.73	2.76	−
N1−P	4.46	3.94	1.90	1.94
N2−H1	1.09	1.05	1.05	1.05
O1−P−O3−O2	131.40	−176.67	−162.67	−165.21

[a] B3LYP calculations with basis sets: O, N, and P (6-31+G*), C (6-31G*), and H (6-31G). [b] Names are defined in Figures 4, 5, and 7.

Starting from **BIMPP**$^{\pm}$**.w** the two pathways of Scheme 3 were evaluated: activation of the coordinated water, to act as the nucleophile, and direct nucleophilic attack of N1 on the P atom. The transition states involved in the two mechanisms are labeled **TS.GB** and **TS.NUC**, respectively, and are shown in Figure 4. Relevant structural details are given in Table 4.

In **TS.GB**, the imaginary frequency observed corresponds to O5−P attack, with simultaneous O4−P bond breaking; N1 modestly activates the water molecule, and H1 strongly stabilizes the leaving group departure through general acid catalysis, with an O4−H1 bond length of 1.66 Å and a quasi planar arylimidazole aromatic system (O1−P−O3−O2 = −176.67°). Furthermore, the strong hydrogen bonding between O3−H1 in **BMIPP**$^{\pm}$**.w** is not observed in **TS.GB** due to the strong O4−H1 hydrogen bond.

For nucleophilic attack, structure **TS.NUC** shows an advanced transition state with a higher degree of bond formation between N1−P (1.90 Å) compared with O5−P in **TS.GB** (2.20 Å) and an O1−P−O3-O2 dihedral angle of −162.67°. The stabilization of the leaving phenoxide group by O4−H1 hydrogen bonding observed in **TS.GB** is absent in **TS.NUC**, with a preferred stabilization of the negative charge at O3, which is hydrogen bonded to H1 (O3−H1 = 1.68 Å) as in **BMIPP**$^{\pm}$**.w**. Aside from the bond making and breaking at the phosphorus center, the

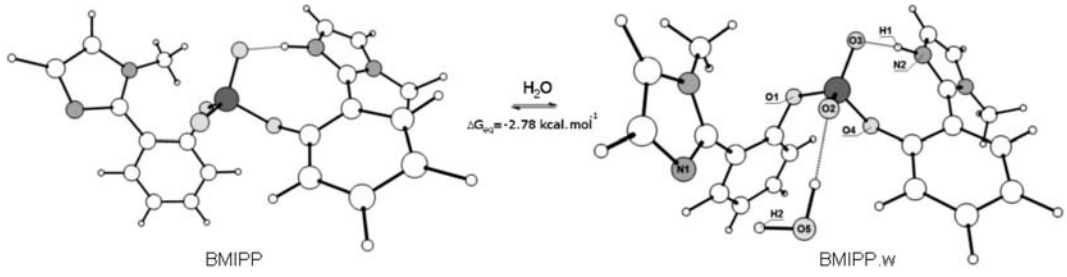

Figure 3. B3LYP gas phase optimized structures of **BMIPP**$^{\pm}$ and **BMIPP**$^{\pm}$**.w** showing the ΔG_{eq} involved in the organic phosphate−water complex formation. The basis set used is given in the Experimental Section.

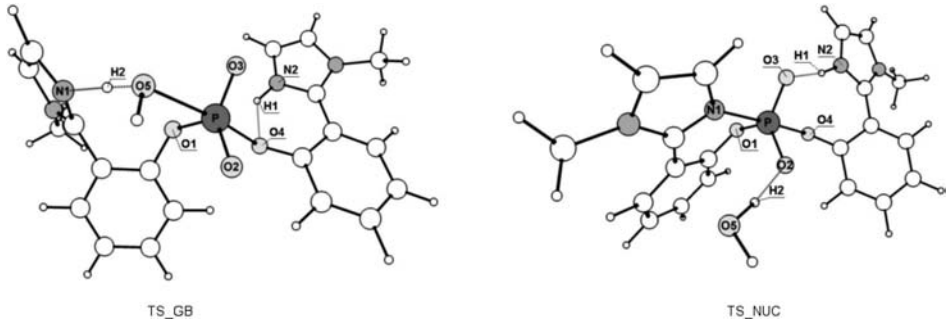

Figure 4. B3LYP gas phase optimized structures of **TS.GB** and **TS.NUC**. The basis set used is given in the Experimental Section.

Table 5. Experimental and B3LYP Gibbs Energy, Enthalpy, and Entropy of Activation for Structures **TS.GB** and **TS.NUC**[a] Energies Relative to **BMIPP**$^{\pm}$**.w**

	$\Delta G^{\ddagger}$/kcal·mol^{-1}	$\Delta H^{\ddagger}$/kcal·mol^{-1}	$\Delta S^{\ddagger}$/cal·mol^{-1}·K^{-1}
Experimental	21.7 ± 1.4[b]	19.0 ± 1.2	−9.0 ± 0.5
TS.GB	28.4	29.2	2.7
TS.NUC	18.9	18.6	−1.2

[a] All quantities calculated at 298.15 K. B3LYP calculations with the following basis set: O, N, and P (6-31+G*), C (6-31G*), and H (6-31G). [b] Calculated at 298.15 K.

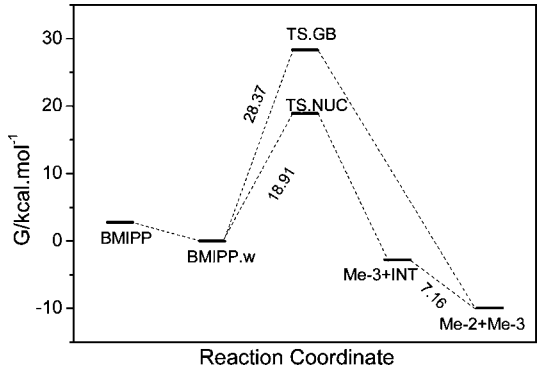

Figure 5. Free energy variation along the reaction coordinates involving **TS.GB** and **TS.NUC**. Energies values relative to **BMIPP**$^{\pm}$**.w**. Structures calculated at the B3LYP level with the following basis sets: O, N, and P (6-31+G*), C (6-31G*), and H (6-31G).

major structural difference between **TS.NUC** and **BMIPP**$^{\pm}$**.w** is the twisting of the imidazole ring needed to put N2 in a reasonable position to attack P.

Although paths **A** and **B** (Scheme 3) are kinetically equivalent, the calculated $\Delta G^{\ddagger}$ is some 9.5 kcal·mol^{-1} lower for **TS.NUC** than for **TS.GB** as shown in Table 5, a result which clearly indicates the nucleophilic pathway as the favored route for the reaction. For reaction via **TS.NUC**, the calculated $\Delta G^{\ddagger}$ is only 2.79 kcal·mol^{-1} lower than the experimental value and the agreement of the calculated $\Delta H^{\ddagger}$ is even closer, differing by only 0.44 kcal·mol^{-1} from the experimental value. Although there is a considerable difference between the experimental and calculated $\Delta S^{\ddagger}$, the theoretical value is in accord with that expected for an intramolecular reaction and the difference is most likely associated with reorganization of solvent molecules, which is not of course addressed by our gas phase calculations.

As shown in Figure 5, the decomposition of **TS.GB** leads to arylimidazole (**Me-3**) + **Me-2**, while **TS.NUC** decomposes to **Me-3** + **INT**. Calculated structures of the reaction products are given in the Supporting Information. The reaction path involving **TS.NUC** is more efficient and results in the formation of **Me-2** + **INT**, which are 7.16 kcal·mol^{-1} higher in energy than the actual reaction products ((**Me-3**) + **Me-2**). Since the phosphorane intermediate was not detected in any of the earlier NMR experiments, the calculations indicate that **INT** decomposes rapidly under mild reaction conditions.

In **TS.NUC**, the water molecule is not directly involved in the bond making−breaking process. Thus, we also modeled the nucleophilic attack of the imidazole group toward P without the assisting H_2O: the results are very similar. Starting from the **BMIPP**$^{\pm}$ zwitterion, $\Delta G^{\ddagger}$ for the N1 attack is 19.57 kcal·mol^{-1}, which is also in excellent agreement with the experimental value (Table 5): the corresponding transition state structure **TS.NUC2** is shown in Figure 6.

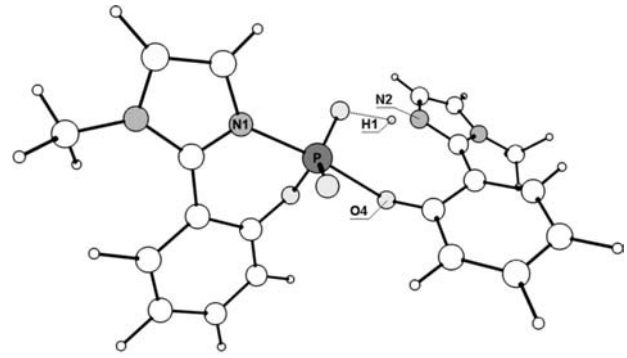

Figure 6. B3LYP gas phase optimized of **TS.NUC2**. The basis set used is given in the Experimental Section.

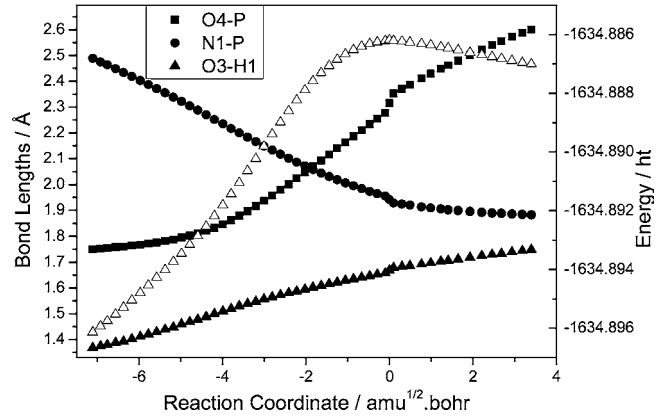

Figure 7. Variations of bond lengths and energies (Δ) along the IRC for the intramolecular nucleophilic attack reaction in **BMIPP**$^{\pm}$ via **TS.NUC2** (Note that H1 is within strong H-bonding distance of O4).

As shown in Table 4, the main bond lengths and angles of **TS.NUC** and **TS.NUC2** are very similar, as is the central bond making−breaking process. Thus (to minimize computational expense) we performed an IRC analysis on **TS.NUC2**: Figure 7 shows the changes in bond lengths involving this structure. The approach of N1 toward P can be seen to be concerted with O4 departure, while H1 is transferred to N2, stabilizing the leaving group.

Mass Spectrometric Measurements. Building on our experience in reaction mechanism studies using MS techniques,[29,30] we applied ESI-MS-(/MS) and LTQ-FT to monitor the course of the hydrolysis of **BMIPP**$^{\pm}$ in aqueous solution. In the ESI-MS process used here, solvated ions are "fished" directly from solution and transferred to the gas phase. The data provide snapshots of the ions present in the reaction solution, which have been shown in numerous cases to reflect accurately the actual ionic composition (see the cited references and a recent Wiley book *Reactive Intermediates: MS Investigations in Solution*, edited by Leonardo S. Santos). After 25 min (4 half-lives) of reaction at pH 6.5 and 60 °C, samples of reaction solution, containing all reagents, intermediates, and products, were transferred directly to the gas phase and detected by

(29) Domingos, J. B.; Longhinotti, E.; Brandão, T. A. S.; Santos, L. S.; Eberlin, M. N.; Bunton, C. A.; Nome, F. *J. Org. Chem.* **2004**, *69*, 7898–7905.
(30) Orth, E. S.; da Silva, P. L. F.; Mello, R. S.; Bunton, C. A.; Milagre, H. M. S.; Eberlin, M. N.; Fiedler, H. D.; Nome, F. *J. Org. Chem.* **2009**, *74*, 5011–5016.

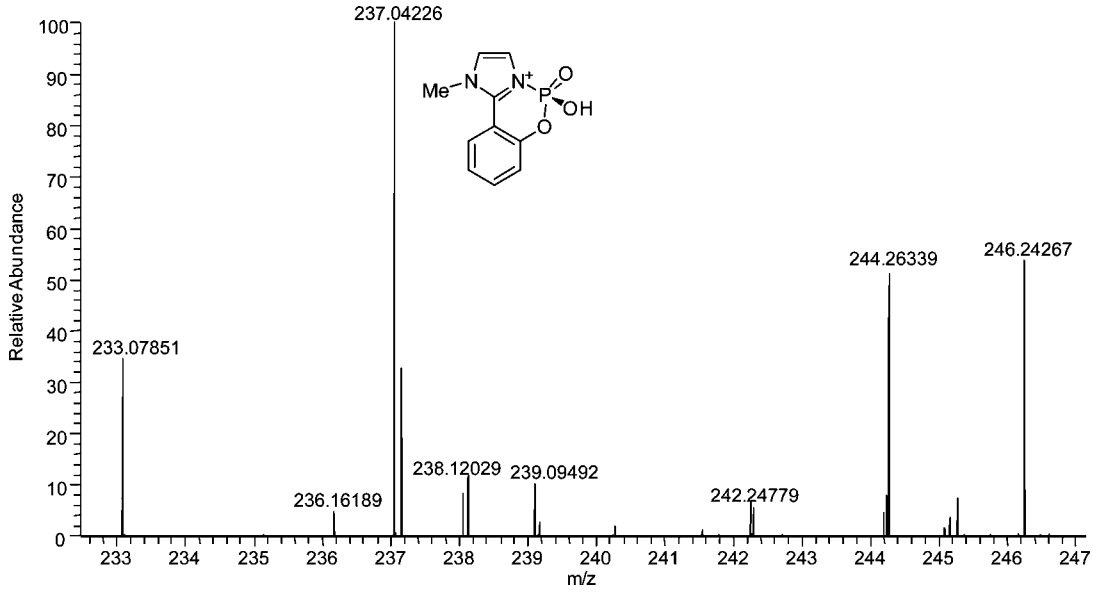

Figure 8. ESI(+) FT-ICR MS after 10 min of hydrolysis of **BMIPP** in aqueous solution at pH 6.5 and 60 °C.

ESI(±)-MS and then the gaseous ionic species transferred to the gas phase were characterized by ESI(±)-MS/MS. Initially,[7] ESI-MS-(/MS) showed a series of the major anions from Scheme 4, which were identified as: (i), the deprotonated form of the reactant **BMIPP** of *m*/*z* 409; (ii) the monoester **Me-2** of *m*/*z* 253; (iii) the phenolate **Me-3** of *m*/*z* 17; and (iv) inorganic P in the form of PO_3^- of *m*/*z* 79 and H_2PO_4 of *m*/*z* 97. No cyclic intermediate (**INT**) could be detected by ESI-MS in either negative or positive ion modes, which does not rule out its formation, since this cyclic species could be relatively unstable. However, some important species could be detected and characterized via collision-induced dissociation in ESI(−)-MS/MS experiments, with the resulting spectra supporting the structural assignments. The ESI(−)-MS/MS of the **Me-2** anion of *m*/*z* 253 *m*/*z* shows that it dissociates almost exclusively to PO_3^- of *m*/*z* 79. Deprotonated **Me-3**, of *m*/*z* 173, dissociates mainly by two routes that lead either to the fragment ion of *m*/*z* 158 by the loss of a methyl radical or the fragment of *m*/*z* 118, most likely by losing 1-methyl-1*H*-azirine (C_3H_5N) to form the 2-cyanophenoxy anion.

To address further the possibility of the intramolecular nucleophilic pathway, ultrahigh resolution and accuracy LTQ FT-ICR MS data, which combine the most advanced Ion Trap and Fourier Transform Ion Cyclotron Resonance technologies, were acquired in both the negative and positive mode. In the negative ion mode, the same anions identified by Q-TOF were detected. In the positive mode (Figure 8), an ion of *m*/*z* 237 was intercepted and assigned to the cyclic intermediate (**INT**). Indeed, the program Xcalibur 2.0 (Thermo Scientific), which calculates molecular composition to within 0.4 ppm, identified $C_{10}H_{24}O_3N_1P_1$ as the most probable composition for the ion of *m*/*z* 237.14. Thus, the hydrolysis of **BMIPP**$^{\pm}$ is seen to involve intramolecular nucleophilic attack by an imidazole group.

Conclusions

We have now studied the hydrolysis of **BMIPP**$^{\pm}$ in considerable depth and have gathered enough evidence to assign the mechanism with some confidence. The kinetic evidence indicates bifunctional catalysis of the hydrolysis of **BMIPP**$^{\pm}$ involving the two imidazole groups, one as the free base, the other as the conjugate acid (paths **A** and **B** of Scheme 3). The imidazolium group clearly acts as a general acid to assist the departure of the leaving group, but the neutral imidazole could be involved either as a general base, catalyzing the attack of water, or directly as a nucleophile, in which case the initial product must be the cyclic phosphoimidazole **INT**. There is no kinetic evidence for the presence of **INT** during the course of the reaction. There are good reasons based on the overall efficiency of catalysis to interpret the kinetic evidence in terms of the nucleophilic mechanism, but these are not sufficient to rule out the general base mechanism pathway (**A** in Scheme 3) completely. The general base catalysis mechanism was preferred initially because it is consistent with the kinetic parameters and because no cyclic intermediate was detected by ESI-MS (in either positive or negative mode) or by NMR (^{1}H and ^{31}P). However, the phosphoryl-imidazolium (P−N$^+$) bond is unstable,[31] so that the nondetection of the intermediate could be the result of its short lifetime, before breaking down to products, which are the same from either mechanism. New calculations strongly favor the nucleophilic mechanism and encouraged us to investigate the possible presence in the reaction mixture of low concentrations of **INT**, using more sensitive ES-MS techniques. The positive result obtained using LTQ-FT (+) (Figure 8), showing that **INT** is indeed present during the course of the reaction, provides unambiguous support for the nucleophilic-IGBC mechanism (path **B** of Scheme 3). Encouraged by the positive identification of **INT** and to obtain positive evidence in the aqueous phase, we are currently studying the stability of a series of phosphoryl-imidazolium (P−N$^+$) derivatives, to obtain better estimates of the expected reactivities of N-phosphoryl imidazolium systems. Though we cannot rule out the possibility of a small contribution from the IGBC pathway, the application of Occam's razor[32] is well justified by the general arguments from catalytic efficiency and the unambiguous indications from our calculations.

(31) Attwood, P. V.; Piggott, M. J.; Zu, X. L.; Besant, P. G. *Amino Acids* **2007**, *32*, 145–156.
(32) Bergson, G.; Linderberg, J. *J. Phys. Chem. A* **2008**, *112*, 4235–4240.

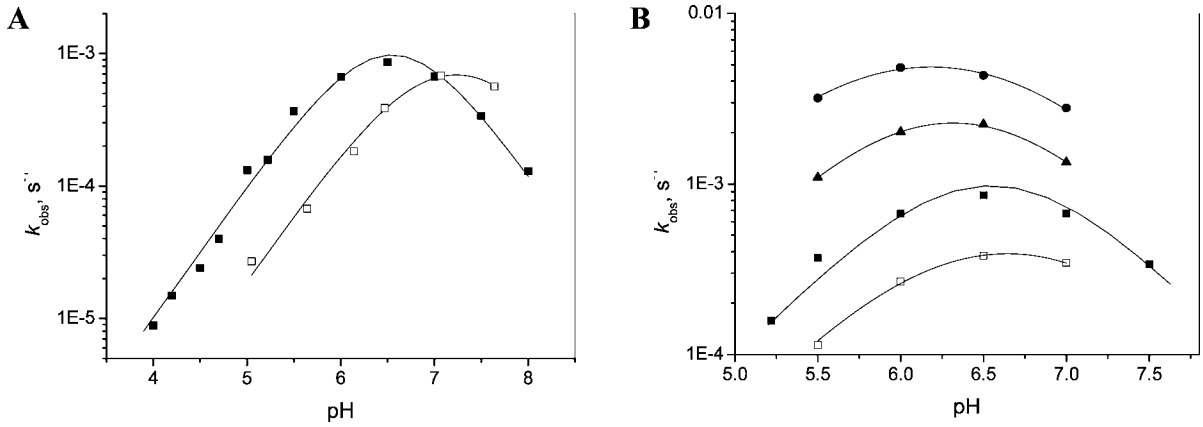

Figure 9. pH−rate profile for the hydrolysis of **BMIPP** in (A) H_2O (-■-) and D_2O (-□-); (B) at 50 °C (-□-), 60 °C (-▲-), 70 °C (-●-), and 80 °C (-■-). The curves show the fits using eq 1, and the parameters obtained are presented in Table 3. The points in H_2O at 60 °C, shown for comparison, are from Figure 1.

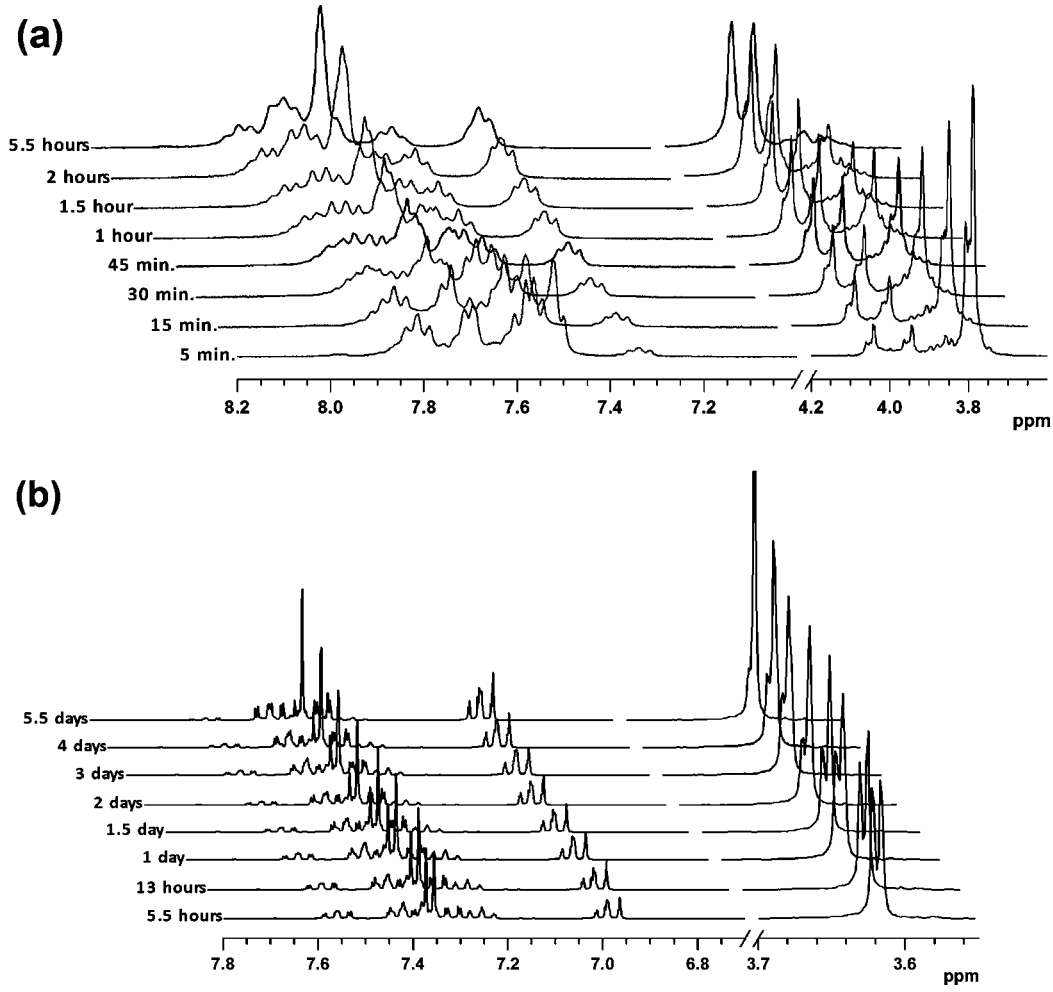

Figure 10. Progressive ^{1}H NMR spectra of the hydrolysis reaction of **BMIPP**. (a) Hydrolysis of **BMIPP** at pD 7.2 and (b) hydrolysis of the intermediate monoester **Me-2** at pD 1.5, in D_2O, at 60 °C. Signals are identified in Table 6.

Experimental Section

Materials. Inorganic salts were of analytical grade and were used without further purification. Liquid reagents were purified by distillation. 1-Methyl-2-(2′-hydroxyphenyl)imidazole (**Me-3**) was prepared by the method of Rogers and Bruice.[8]

Synthesis of Bis(2-(1-methyl-1*H*-imidazolyl)phenyl)phosphate (BMIPP). A solution of PCl_5 (600 mg, 2,87 mmol) in $CHCl_3$ (15 mL) was added dropwise to a $CHCl_3$ solution of 1-methyl-2-(2′-hydroxyphenyl)imidazole (500 mg, 2.87 mmol in 15 mL) in an ice−water bath, under argon. The mixture was stirred at room temperature for 120 min. Water was then added (0.25 mL), and the mixture was left to react overnight. The solvent was removed under reduced pressure, and methanol (5 mL) and water (3 mL) were added to the resulting crude oil. Fine white crystals (370 mg, 51%) of **BMIPP** were obtained immediately. ^{13}C NMR (100 MHz, D_2O, internal reference TSP) δ 149.91, 141.57, 134.49, 131.74,

Table 6. NMR Spectra of the Species in the Hydrolysis Reaction of **BMIPP**, in D_2O at 60 °C

Compound	^{1}H NMR δ (ppm)	^{31}P NMR δ (ppm)
BMIPP (pD = 7.2)	δ 3.79 (s, 6H, Me), 7.5−7.6 (m, 8H, Ar), 7.70 (d, 2H, Ar), 7.81 (t, 2H, Ar)	−10.38
Me-2 (pD = 7.2)	δ 4.03 (s, 3H, Me), 7.5−7.8 (m, 5H, Ar), 7.88 (t, 1H, Ar)	1.22
Me-2 (pD = 1.5)	δ 3.62 (s, 3H, Me), 7.5−7.8 (m, 5H, Ar), 7.56 (t, 1H, Ar)	−4.30
Me-3 (pD = 7.2)	δ 3.97 (s, 3H, Me), 7.3−7.4 (m, 2H, Ar), 7.5−7.8 (m, 4H, Ar)	
Me-3 (pD = 1.5)	δ 3.62 (s, 3H, Me), 6.9−7.0 (m, 2H, Ar), 7.30 (d, 1H, Ar), 7.34 (s, 2H, Ar), 7.41 (t, 1H, Ar)	
P_i		0.57

125.28, 124.02, 120.56, 119.22, 114.41, 34.99; ^{1}H NMR (400 MHz, D_2O, internal reference TSP) δ 3.48 (s, 6H, CH_3), δ 7.13 (d, 2H, J_{AB} = 8.4 Hz), δ 7.23 (dt, 2H, J_{CB} = 7.6 and J_{CD} = 7.6 Hz), δ 7.30 (dd, 4H, J_{FG} = 5.2 and J_{GF} = 5.2 Hz), δ 7.37 (d, 2H, J_{DC} = 7.6 Hz), δ 7.48 (dt, 2H, J_{BC} = 7.6 and J_{BA} = 8.4 Hz). ^{31}P NMR (81 MHz, D_2O, external reference H_3PO_4 85%) δ −10.38 ppm, s; *m*/*z* (ESI-MS) 409,1720 $C_{20}H_{18}N_4O_4P$ requires 409.1066

Potentiometric Titrations. The pK_a values of **BMIPP** were determined using a digital pH meter and a combined glass electrode, equipped with an automatic buret. Titrations were performed in a 150 mL thermostatted cell, under N_2 at 25.0 °C, at ionic strength 0.1 M KCl, and [**BMIPP**] = 1.0 mM (initial). The solution was titrated with small increments of 0.1008 M CO_2-free KOH. All precautions were taken to eliminate carbonate and CO_2 during the titration. The program BEST7[33] was used to calculate the dissociation constants, using the value −13.78 for pK_w.

Kinetics. Reactions of **BMIPP** and **Me-2** were followed spectrophotometrically by monitoring the appearance of 1-methyl-2-(2′-hydroxyphenyl)imidazole (**Me-3**) at 290 nm. Reactions were started by adding 20 μL of 10 mM stock solutions of the substrate in water (pH = 10: stored in a refrigerator to minimize hydrolysis) to 3 mL of aqueous solution in quartz cuvettes, to give a final concentration of the substrate of 66.7 μM. The temperatures of the reaction solutions in the cuvettes were controlled with a thermostatted water-jacketed cell holder, and ionic strengths were kept constant at 1.0 M with KCl. Absorbance versus time data were stored directly on a microcomputer, and observed first-order rate constants, k_{obs}, were calculated from linear plots of $\ln(A_\infty - A_t)$ against time for at least 90% of the reaction using an iterative least-squares program; correlation coefficients were better than 0.999 for all kinetic runs. The pH was maintained with 0.01 M buffers of $CH_2ClCOOH$ (pH 2−3), HCOOH (pH 3−4.5), CH_3COOH (pH 4−5.5), and NaH_2PO_4 (pH 5.5−6.0). In solutions where [HCl] > 0.5 M, the reactions were self-buffered with no ionic strength correction. Reactions at pD 7.2 and pD 1.5 were also followed by NMR to follow the appearance of products and disappearance of reagents.

Since the pH−rate profile for the hydrolysis of **BMIPP**$^{\pm}$ is bell shaped (at all temperatures investigated and in both H_2O and D_2O), the solvent deuterium kinetic isotope effect and activation parameters were calculated from the rate constants k_{3d} obtained by fitting experimental data in the range of pH 5.5−8.0, as shown in Figure 9A and B. The values obtained (including the acid dissociation constants pK_{a2} and pK_{a3}) are shown in Table 3. The kinetic isotope effect is defined by k_{3H_2O}/k_{3D_2O}, and activation parameters were calculated by plotting $\ln(k_{3d}/T)$ vs $1/T$, according to Eyrings' equation.[13]

Mass Spectrometric Measurements. To identify intermediates and reaction products of **BMIPP** hydrolysis, direct infusion electrospray ionization mass spectrometry was performed using a hydrid triple quadrupole linear ion-trap mass spectrometer.[30] The typical electrospray ionization (ESI-MS) experiment involved 1 mL of aqueous 1×10^{-6} M **BMIPP** solution at pH 6.5. A microsyringe pump delivered the reagent solution into the ESI source at a flow rate of 10 μL/min. ESI and the QqQ (linear trap) mass spectrometer were operated in the negative-ion mode. Main conditions: curtain gas nitrogen flow of 5 mL min^{-1}; capillary voltage of −3500 eV; cone voltage of −30 eV. Some of the main anionic species detected by ESI-MS were subjected to ESI-MS/MS by using collision-induced dissociation (CID) with nitrogen, with collision energies ranging from 5 to 45 eV for the best dissociation yields. For accurate mass measurements of possible intermediates, direct infusion automated chip-based nano-ESI-MS were performed on a Triversa NanoMate 100 system in both the positive and negative ion modes. Samples were loaded into 96-well plates (total volume of 100 μL in each well) and analyzed by a 7.2T LTQ FT Ultra mass

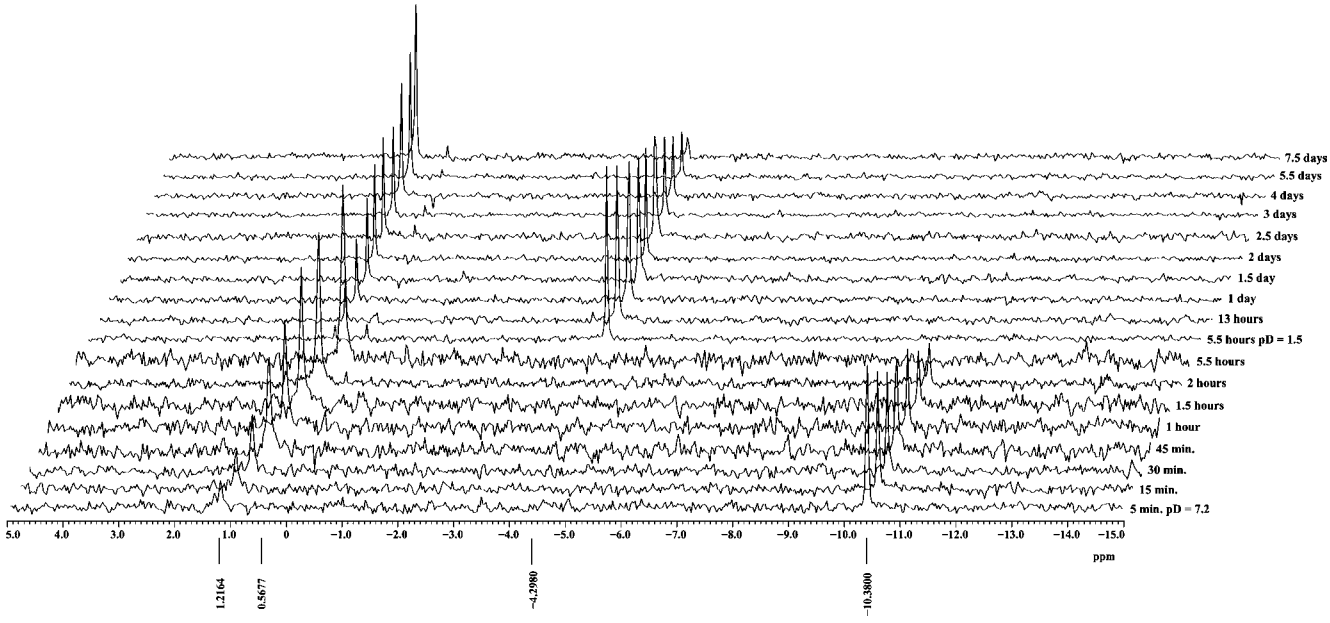

Figure 11. Progressive ^{31}P NMR spectra for hydrolyses of **BMIPP** (pD 7.2, 5 min to 5.5 h) and **Me-2** (pD 1.5, 5.5 h to 7.5 days), in D_2O at 60 °C. Signals are identified in Table 6.

spectrometer. ESI general conditions were as follow: gas pressure of 0.3 psi, capillary voltage of 1.55 kV, and a flow rate of 250 nl min^{-1}.

NMR Spectra. ^1H and ^{31}P NMR spectra taken at regular time intervals were recorded on a spectrometer (300 MHz for ^1H) using D_2O as solvent. The pD values of the solutions were corrected considering $pD = pH_{read} + 0.4$ at 25 °C. Spectra were recorded at regular intervals at 60 °C during **BMIPP** hydrolysis at pD 7.2, while the spectroscopic data for the much slower hydrolysis of the **Me-2** intermediate at 60 °C and pD 1.5 were collected at 25 °C. ^1H and ^{31}P chemical shifts are referred to sodium 3-(trimethylsilyl) propionate (TSP, internal) and H_3PO_4 85% (external reference), respectively. The relaxation delay was 1 s for all acquisitions.

Significant changes in the ^1H NMR spectra are observed in the *N*-methyl region (Figure 10). At pD 7.2 the disappearance of the **BMIPP** peak at 3.79 ppm is accompanied by the appearance of two new signals at 4.03 and 3.97 ppm, which are assigned to **Me-2** and **Me-3**, respectively. At pD 1.5 these two peaks are displaced upfield to approximately 3.62 ppm and the hydrolysis of **Me-2** affords a single peak of product **Me-3**. The assignments for the aromatic region are less obvious, but the spectra at pD 7.2 clearly show the appearance of peaks at 7.88 and 7.34 ppm for **Me-2** and **Me-3**, respectively. As in the aliphatic region, these peaks are also displaced upfield at pD 1.5, where the hydrolysis of **Me-2** is observed as the disappearance of the peak at 7.56 ppm and the appearance of the product of **Me-3** at 6.99 ppm.

The ^{31}P NMR spectra offer a clearer view of **BMIPP** hydrolysis (Figure 11). At pD 7.2, the **BMIPP** peak at −10.4 ppm disappears over time, giving the **Me-2** monoester at 1.22 ppm. This peak is displaced at pD 1.5 to −4.30 ppm, and hydrolysis of **Me-2** gives inorganic phosphate ($\mathbf{P_i}$: chemical shift 0.57 ppm under the conditions).

Computational Methods. All computational calculations were performed using Gaussian 03[34] at the DFT level employing the hybrid B3LYP[35−38] functional. The P, N, and O atoms were described by the 6-31+G(d) basis set, and C and H by 6-31G(d) and 6-31G basis sets, respectively. The geometry optimizations were carried out in the gas phase, and water solvation free energies (ΔG^{solv}) were estimated using PCM[39,40] on single-point calculations, with the molecular cavity computed, including explicit hydrogens, using the UFF radius.[41] Tables of Cartesian coordinates and thermochemistry data are presented in sections 3.1 to 3.9 of the Supporting Information.

All reactants and transition states were properly characterized in force constant calculations by the absence or presence of a single negative eigenvalue, respectively, and all thermodynamic parameters were converted from a 1 atm standard state into the standard state of molar concentration.[42,43]

For the unassisted nucleophilic attack pathway (Path **B**, Scheme 3) intrinsic reaction coordinate (IRC) computations[44] were performed, at the same level of theory described above, starting from the optimized transition state structure (**TS.NUC**), using a step length of 0.10 $(a.m.u)^{1/2}$ bohr.

Acknowledgment. We thank INCT-Catálise and the Brazilian foundations CNPq, FAPESC, FAPESP, and Capes for financial assistance.

Supporting Information Available: Bunnett plot for acid hydrolysis of **BMIPP**. Tables of the Bunnett plot, pH rate profile for **BMIPP** and **Me-2**, and kinetic data in D_2O and at different temperatures. pH rate profile for the reaction of **BMIPP** with nucleophiles with data table. Potentiometric titration data and species distribution. Tables of Cartesian coordinates and thermochemistry data from computational calculations. Complete ref 34. This material is available free of charge via the Internet at http://pubs.acs.org.

JA1034733

(33) Martell, A. E. S., Z. M.; Motekaitis, R. J. *NIST Critical Stability Constants of Metal Complexes Database: NIST Standard Reference Database 46*; NIST: Gaithersburg, MD, 1993.
(34) Frisch, M. J. *Gaussian 98*, revision D.01; Gaussian, Inc.: Pittsburgh, PA, 2004.
(35) Becke, A. D. *J. Chem. Phys.* **1993**, *98*, 5648–5652.
(36) Lee, C. T.; Yang, W. T.; Parr, R. G. *Phys. Rev. B: Condens. Matter* **1988**, *37*, 785–789.
(37) Vosko, S. H.; Wilk, L.; Nusair, M. *Can. J. Phys.* **1980**, *58*, 1200–1211.
(38) Stephens, P. J.; Devlin, F. J.; Chabalowski, C. F.; Frisch, M. J. *J. Phys. Chem.* **1994**, *98*, 11623–11627.
(39) Tomasi, J.; Mennucci, B.; Cammi, R. *Chem. Rev.* **2005**, *105*, 2999–3093.
(40) Tomasi, J.; Persico, M. *Chem. Rev.* **1994**, *94*, 2027–2094.
(41) Rappe, A. K.; Casewit, C. J.; Colwell, K. S.; Goddard, W. A.; Skiff, W. M. *J. Am. Chem. Soc.* **1992**, *114*, 10024–10035.
(42) Benson, S. *Thermochemical Kinetics*; Wiley: New York, 1968.
(43) Rastelli, A.; Bagatti, M.; Gandolfi, R. *J. Am. Chem. Soc.* **1995**, *117*, 4965–4975.
(44) Fukui, K. *Acc. Chem. Res.* **1981**, *14*, 363–368.